A Flat Heat Pipe Architecture Based on Nanostructured Titania

Changsong Ding, Gaurav Soni, Payam Bozorgi, Brian D. Piorek, Carl D. Meinhart, and Noel C. MacDonald

***Abstract*—A novel 3 cm × 3 cm × 600 μm-thick Ti-based flat heat pipe is developed for Thermal Ground Plane (TGP) applications. The Ti-based heat pipe architecture is constructed by laser welding two microfabricated titanium substrates to form a hermetically sealed vapor chamber. The scalable heat pipes' flat geometry facilitates contact with planar heat sources, such as microprocessor chip surfaces, thereby reducing thermal contact resistance and improving system packaging. Fluid transport is driven by the wicking structure in the TGP, which consists of an array of Ti pillars that are microfabricated from a titanium substrate using recently developed high-aspect-ratio Ti processing techniques [1]. The hydrophilic nature of the Ti pillars is increased further by growing ∼200-nm hairlike nanostructured titania of the pillar surfaces. The resulting super hydrophilic wick offers the potential to generate high wicking velocities of ∼27.5 mm/s over distances of 2 mm. The experimental wetting results show a diffusive spreading behavior that is predicted by Washburn dynamics [2]. The maximum effective thermal conductivity of a heat pipe is directly related to the speed of capillary flow of the working fluid through the wick and is measured experimentally in the first-generation device to be $k = 350$ W/m · K. A dummy TGP with a cavity volume of ∼170 μL was used to test the hermiticity level of the laser packaging technique. The device gave a 0.067% of water loss based on ∼60 μL of charged water at 100 °C in air for over a year. [2009-0303]**

***Index Terms*—Heat pipe, nanostructure, Thermal Ground Plane (TGP), titanium, vapor chamber.**

I. Introduction

COOLING devices such as heat sinks, fans, and heat pipes have long been utilized for cooling microprocessor chips [3]. Heat pipes have been of particular use in cooling power-intensive chips because of their high thermal conductivity and their capacity to carry high amounts of heat [4]. Heat pipes are composed of the following three components: a hermetically sealed cavity, a working fluid, and a wick structure on the internal walls of the cavity. Different kinds of materials such as biporous copper [5], sintered copper [6], carbon nanotubes [7], microstructures with different topologies [8] and patterns [9], and micromachined channels have been investigated for micro heat pipes for their wicking functions. The hermetically sealed cavity is filled with a working fluid such as water or ammonia etc., depending on the heat load and design operating temperatures. The high heat-carrying capacity of a heat pipe is due to the latent heat and transport of the working fluid. During operation, the working fluid evaporates by absorbing heat into a hot region (heat source) of the heat pipe and flows as a vapor toward a cold region (heat sink) where condensation then occurs due to the cooler temperature. A very fine wick structure on the internal wall of the heat pipe draws the condensate from the cold region to the hot region using capillary action.

This transport cycle is continuous within a heat pipe, thereby transporting large amounts of heat. Since the latent heat of evaporation of the working fluid is high relative to sensible heat, heat pipes can transport much higher amounts of heat than what can be conducted through a solid rod of the same dimension of solid materials.

Heat pipes are an essential component of contemporary laptop cooling systems because of the high power dissipated by modern microprocessor chips. Generally, heat pipes are cylindrical in shape and are made of copper, with a fine copper wire mesh attached to the internal walls. Such cylindrical heat pipes do not establish good thermal contact with the flat surfaces on microprocessor chips, and they are not easily packaged in a planar geometry. Flat heat pipes are known as vapor chambers, and they suffer from poor fluid transport efficiency and thereby have a low thermal conductivity compared to cylindrical heat pipes.

Titanium offers many advantageous properties relative to other micromechanical materials, including high fracture toughness and excellent corrosion resistance. Using recently developed micromachining techniques based on Cl_2/Ar dry etching [1], [10], high-aspect-ratio structures with micrometer-scale and nanoscale features are made out of titanium foil/substrates. The etched substrates can then be bonded or welded to other substrates to enable the realization of complex multilayered devices. These foil substrates can be obtained in thicknesses ranging from 10 μm to many hundred micrometers, with minimal intrinsic residual stress. The high modulus and weldability of titanium allow greater design flexibility than what is possible with other materials such as ceramics, low modulus metals, and deposition-based thin films, where residual stresses can cause undesirable deformation of the device structures [11].

Titanium is a unique material for Thermal Ground Plane (TGP) in that it can be microfabricated and oxidized to create

Manuscript received December 2, 2009; revised April 13, 2010; accepted May 3, 2010. Date of publication June 14, 2010; date of current version July 30, 2010. This work was supported by the TGP program from the Microsystems Technology Office, Defense Advanced Research Projects Agency, under Grant N66001-08-1-2035. A portion of this work was done in the UCSB nanofabrication facility, which is part of the NSF-funded NNIN network. Subject Editor R. T. Howe.

C. Ding is with the California NanoSystems Institute, University of California, Santa Barbara, CA 93106-6105 USA (e-mail: changsong_ding@yahoo.com).

G. Soni, P. Bozorgi, C. D. Meinhart, and N. C. MacDonald are with the Department of Mechanical Engineering, University of California, Santa Barbara, CA 93106-9560 USA.

B. D. Piorek is with SpectraFluidics, Inc., Santa Barbara, CA 93117 USA, and also with Gas Reaction Technologies, Inc., Santa Barbara, CA 93110 USA.

Color versions of one or more of the figures in this paper are available online at http://ieeexplore.ieee.org.

Digital Object Identifier 10.1109/JMEMS.2010.2051019

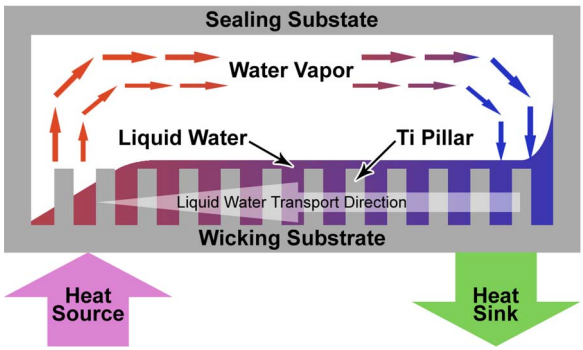

Fig. 1. Schematic of the Ti-based TGP architecture. The overall device thickness is less than 1 mm. The bottom substrate is a 250-μm-thick Ti. The super hydrophilic substrate is a combination of Ti and TiO_2 and is 50 μm in height. The vapor cavity is 100 μm tall. The sealing structure is 200 μm thick.

nanoscale features. In addition, Ti can be macromachined and laser welded to produce a hermetically sealed chamber. The high fracture toughness of Ti makes it an excellent material for fabrication of thin, lightweight, flexible, and robust heat pipes.

The current work demonstrates the proof of concept for fabrication and performance of a Ti-based flat heat pipe (vapor chamber) for cooling planar geometries. This approach incorporates microfabricated Ti pillars that are oxidized to produce nanoscale features to create a super hydrophilic wicking structure. The wick can be optimized further to increase fluid transport, and thereby, it achieves a high heat-transfer performance.

II. Device Geometry

A schematic of the first-generation TGP is shown in Fig. 1. The device is formed by microfabricating Ti pillars from a Ti wafer. A second substrate is laser welded to the first substrate to form a hermetically sealed vapor chamber. The overall thickness is approximately 600 μm, and it has a lateral size of 3 cm $\times$ 3 cm. The lateral size can be readily extended to larger sizes in future designs. The overall weight of the device is measured to be 3.4 gm. A wicking structure is formed from Ti pillars that have a diameter of 5 μm, a center-to-center pitch of 10 μm, and a height of 50 μm. These Ti pillars are oxidized to form nanostructured titania (NST) with characteristic dimensions of approximately 200 nm.

Water is used as the working fluid. During operation, heat is applied to the wicking substrate, causing evaporation. The water vapor is transported to a cold region and is condensed by rejecting heat with a heat sink. The condensed water is then wicked to the evaporating region. This process is continuous during the TGP operation.

III. Fabrication Process

Bulk titanium processing techniques have been developed since 2001 for harsh environment microsystems such as mirrors [1], electrodes [12], and relays [13]. Argon and chlorine are usually used for dry etching of Ti [1], [10]. For the current TGP device, we use well polished commercial grade 1 (CP1) Ti substrates. The fabrication process for making Ti pillars begins with the SiO_2-masked deep etching of a 300-μm-thick

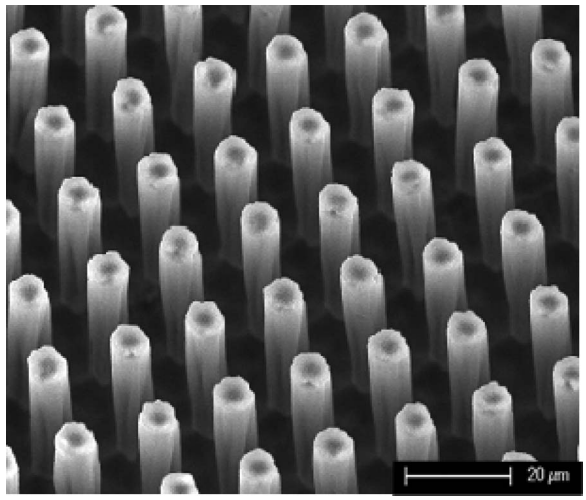

Fig. 2. SEM photograph of the deep-etched bulk Ti pillar array. The pillars have a diameter of 5 μm, a center-to-center pitch of 10 μm, and a height of 50 μm.

Ti substrate using inductively coupled plasma etch in an Ar/Cl_2 ambience. The SiO_2 layer is approximately 3 μm thick. After deep etching is complete, the sample is oxidized in a 30% solution of hydrogen peroxide at 83 °C to obtain the NST hair at the pillar surfaces and the bottom floor surface. NST fabrication, however, is a challenging task, which poses several difficulties. For example, peeling of the NST layer from the Ti surface is often observed when the sample is dipped into hydrogen peroxide immediately after the deep etch step. We believe that it is the $TiCl_x$ passivation layer and the native oxide which inhibit the robust formation of NST. To minimize this problem, we apply an isotropic etch to remove the sidewall passivation layer and contaminants. A high-pressure plasma system, which etches away both the top SiO_2 masking material and the sidewall passivation layer and contaminants, is ideal for this purpose. This etch is realized using a Technics PE IIA plasma etcher (100 kHz RIE) with a $CF_4 : O_2$ chemistry (85 : 15). With this system, an oxygen cleaning procedure (100 W, 300 mtorr, and 1 min) is first applied to the samples to remove the hydrocarbon that may originate from air; then, the $CF_4 : O_2$ chemistry (85 : 15 sccm) is applied (300 W, 300 mtorr, and 15 min) to etch away the top masking material and the side wall passivation layer/contaminants and to expose the fresh Ti surface. Following this etching step, the same oxygen cleaning procedure is applied again to remove the possible CF_4 accumulation on the pillar sidewalls. A very thin layer of TiO_2 may form on the sample surfaces. However, it does not affect NST formation in the following oxidization procedure.

An SEM image of the microscale pillars is shown in Fig. 2. A close-up view of the NST hair on a pillar surface is shown in Fig. 3. The NST film enhances the local wetting of the Ti posts. The wicking structure has length scale ranges of 50-μm high posts, 5-μm diameters, and $\sim$200-nm NST hairs. The range of length scales enhances the wetting characteristics of the wicking structure and is a key for optimal TGP performance.

As mentioned earlier, the NST film enhances the local wetting of the Ti posts. Once wetted, the micropillars create a capillary action over the centimeter length scale. Such a combination of multiple length scales produces a super hydrophilic structure.

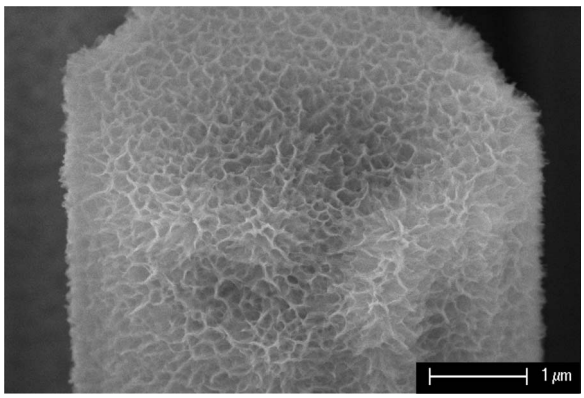

Fig. 3. SEM image of the Ti microstructure. The Ti pillars have a height of 50 μm and a diameter of 5 μm, and they are etched into a Ti substrate with a 5-μm gap. Ti is oxidized to produce ~200-nm hairlike NST. The hairlike structure enhances wetting of Ti pillars.

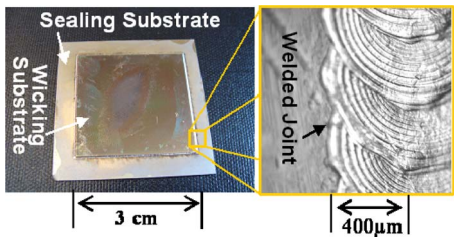

Fig. 4. (Left) Photograph of the first-generation Ti-based TGP. The two Ti substrates are laser welded to form a hermetically sealed vapor chamber. A small quantity of water is sealed within the vapor chamber. (Right) Close-up of the microscale laser weld that joins the two Ti substrates.

IV. Device Packaging Using Laser Welding

For continuous operation, the working fluid and the wick structure must be hermetically sealed in the vapor cavity. The performance of the TGP depends significantly on the quality of packaging. A major problem with the packaging techniques used conventionally for microfabrication, such as high-temperature thermocompression and flip-chip bonding, is the degradation of reliability, which is caused by the excess stress due to thermal mismatch. In order to eliminate the stresses that occur at high temperature, we take a different approach by applying a pulsed laser as a local and rapid heat source to locally weld the Ti substrates, instead of bonding the substrates by heating the entire device.

A pulsed Nd:YAG laser (neodymium-doped yttrium aluminum garnet; Nd : $Y_3Al_5O_{12}$) with a wavelength of 1064 nm was applied as a heat source to locally weld a 30 mm × 30 mm titanium square lid to a titanium substrate (shown in Fig. 4). The applied laser parameters are enumerated in Table I. The hermiticity of the packaged device achieved the leaking rate of 10^{-11} std cm^3/sec using the helium leaking method.

A hole (1.8 mm in diameter) was drilled into the welded package for water charging. The cavity was charged with a measured quantity of water at atmospheric pressure. The quantity of water was judiciously chosen to fill the pores up to the top of the pillars under atmospheric pressure at 100 °C. After adding water, the inlet hole was covered with a small 3 mm × 3 mm piece of Ti and was sealed with an epoxy-based adhesive to form the fully encapsulated TGP device. A laser-sealed (epoxy free) prototype for hermiticity test is shown in the latter part of this paper. By laser welding a patch to seal the charging hole, the degassing issue of epoxy will be avoided. We expect it to be more reliable either by sealing with laser welding or by capping necessary charging tubes with Swagelok end caps.

TABLE I
Laser Parameter Applied for Welding the TGP Device

Laser Parameter	Parameter Value
Laser Power / pulse	1.5 J
Pulse Frequency	18 Hz
Welding spot speed	2mm/sec
Laser welding spot	Circle with 400μm diameter

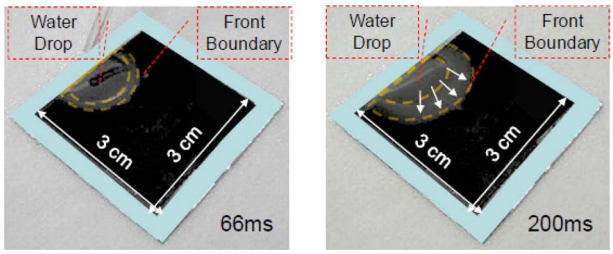

Fig. 5. Hydrophilic nature of the wick was tested by placing a drop of water at the edge of the wicking substrate. The drop of water collapsed and traveled among the pillar arrays. The left figure shows the wetting profile after 66 ms, and the right figure shows the wetting profile at 200 ms.

V. Wetting Performance of the TGP

Washburn [2] originally analyzed the dynamics of capillary flow through a circular tube. By balancing surface tension forces with viscous resistance, he showed that the wetting speed can be written as

$$\frac{dx}{dt} = \frac{r\gamma\cos\theta}{4\eta}\frac{1}{x} \tag{1}$$

where x is the length of the penetration, t is the period of the penetration, r is the radius of the capillary, γ is the surface tension of water, η is the viscosity of water, and θ is the contact angle.

An important feature of this equation is that the wetting velocity scales as x^{-1}. The penetration length can be calculated by integrating (1), and it is shown to increase with the square root of time $x = (Dt)^{1/2}$, where D is the dynamic coefficient. A high dynamic coefficient is preferred for the wicking structure, as this performance metric is directly related to heat transport in the TGP.

The wetting characteristics of the wicking structure (i.e., dynamic coefficient) was measured experimentally. A drop of DI water was placed at the edge of the wicking substrate at room temperature. Once in contact with the surface, the droplet collapsed into the wicking substrate and traveled through the pillar array.

Fig. 5 shows two snapshots recorded during the wetting experiment. The flow of water through the pillars was recorded with a digital camera at 15 frames per second, and the front boundary of water was tracked. The front boundary travels

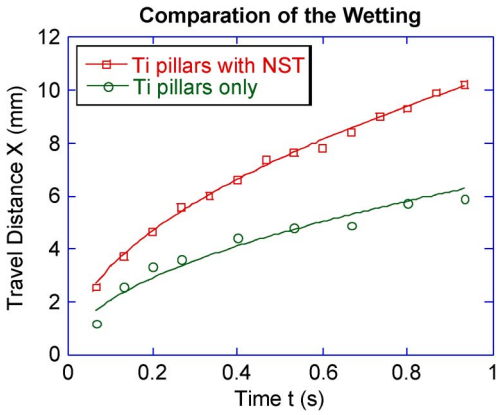

Fig. 6. Length of the wetted region as a function of time. The symbols are the experimental data, while the solid line is the least squares fit of $x = 10.5 \times 10^{-3} t^{1/2}$ for pillars with NST and $x = 6.5 \times 10^{-3} t^{1/2}$ for Ti pillars without NST.

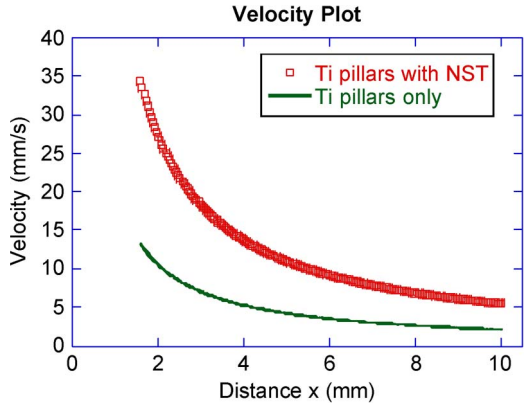

Fig. 7. Velocity plot of Ti pillars and NST-coated Ti Pillars using (3). The wetting velocity for the NST-coated pillars is 160.95% higher than just Ti pillars. The wetting speed for the NST pillars is ~25 mm/s at a distance of 2 mm away from the water drop.

approximately 10 mm in 1 s. The distance traveled by water (i.e., the travel distance of the wetted region) as a function of time is shown in Fig. 6.

A curve of the form $x^2 = Dt$ was fitted to the data for Ti pillars and NST-coated Ti pillars. The results show that $D = 4.225 \times 10^{-5}$ m^2 s^{-1} for Ti pillars (data not shown). When NST is coated on the Ti pillars, the dynamic coefficient D increased by 160.95% to

$$x^2 = Dt = 1.1025 \times 10^{-4} t. \tag{2}$$

The agreement between the experimental data and the curve fit shown in Fig. 6 indicates that the flow distance follows a square root scaling in time. Therefore, we conclude that the wetting in the Ti and NST/Ti pillar array behaves according to Washburn dynamics due to the diffusive wetting nature.

The experimental value of the liquid flow speed dx/dt was determined by differentiating (2), such that

$$\frac{dx}{dt} = \frac{5.5125 \times 10^{-5}}{x}. \tag{3}$$

The wetting velocity $dx/dt = D/2x$ is proportional to the inverse of the penetration distance and is shown in Fig. 7 as a function of time for Ti pillars and NST-coated Ti pillars. Similarly, the wetting velocity profile for the Ti pillars is derived to be $dx/dt = 2.12e - 5/x$. The flow speed decreases $\sim x^{1/2}$. The velocity for the NST/Ti pillars is ~27.5 mm/s at a penetration distance of 2 mm, but it decreases to only 5.5 mm/s at a penetration distance of 10 mm. Literature data profiles are needed for wetting speed comparisons to other wicking materials such as porous copper, carbon nanotubes, and microstructures.

The Washburn equation was originally derived for a circular tube, with r being the radius [2]. The titanium wicking material has a 5 μm × 50 μm feature geometry gap among the pillars. By assuming that we can use $r = 2.5$ μm (half of the gap), that the contact angle is very close to zero, and that water properties are at room temperature, the Washburn equation (1) predicts a wetting velocity profile to be $dx/dt = 1.01e - 4/(2x)$. This dynamic coefficient result is ~8.2% larger than the measurement from NST wicking material.

VI. Heat Transport Performance of the TGP

The rate of heat transport in the TGP is proportional to the rate of evaporation of the working fluid under steady-state conditions

$$\frac{dm_e}{dt} = \frac{dq}{dt}\frac{1}{h_{fg}} \tag{4}$$

where dq/dt is the power input and h_{fg} is the latent heat of evaporation of the fluid.

The mass flow rate of capillary flow through the wick structure is given by

$$\frac{dm_c}{dt} = \rho \nu A_p \tag{5}$$

where ρ is the density of the fluid, ν is the wicking speed [given by (3)], and A_p is the cross-sectional area occupied by the fluid in the wick, which is a function of x. By assuming a triangular profile of the fluid in the wick, A_p is equal to the cross-sectional area by taking half of the pillar height.

The rate of heat transported by the TGP can be calculated by combining (4) and (5)

$$\frac{dq_{\max}}{dt} = \rho h_{fg} \nu A_p. \tag{6}$$

Substituting the wicking speed ν using the modified Washburn equation yields

$$\frac{dq_{\max}}{dt} = \rho h_{fg} \frac{D}{2} \frac{A_p}{L} \tag{7}$$

where L is the length scale over which the heat is transported. The heat-carrying capacity decreases with the length of the heat pipe. For liquid water at 100 °C, we obtain $h_{fg} = 2256.9$ kJ/kg and $\rho = 958.27$ kg/m^3. The speed of capillary flow observed in our experiments (at room temperature) is in the range of 2–25 mm/s (Fig. 7) for the first 10-mm range. By assuming that the wicking material begins to dry out at a small region near the heat source, we calculate the heat-carrying capacity for a high representative velocity of 20 mm/s. The combined pore cross-sectional area can be found in the following way: Since the pore width and the diameter of the pillar are equal, the combined width of the pores is half of the TGP width (which

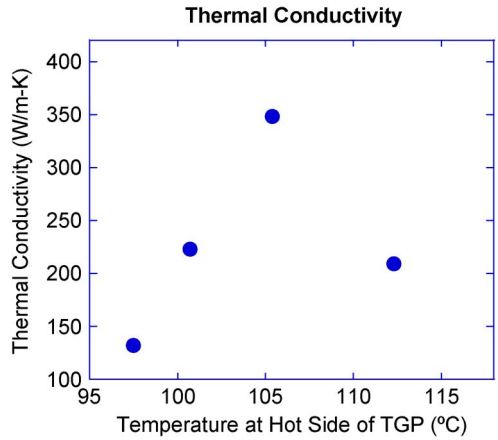

Fig. 8. Effective thermal conductivity of the TGP as a function of the temperature of the heat source. The maximum value was determined to be $\sim$350 W/m · K.

is 3 cm). The height of the pores is about 50 μm. This yields a combined cross-sectional area of 7.5×10^{-7} m^2. Substituting these values in (6) yields a characteristic rate of heat transfer of $dq/dt \approx 18.25$ W.

We have performed experiments which demonstrate the current TGP's performance as a function of the heat source temperature. In these experiments, solid copper bars were used to transfer heat into and out of the TGP. The interfacial area of the bars was matched to the area of the hot and cold regions of the TGP, which was 0.5 cm by 3 cm. A Kapton thin-film heater (McMaster–Carr, item 7980T11) heated the copper bar used for heat injection. The power applied to the Kapton heater was controlled by a variac driven at 120 V and 60 Hz. The distal end of the copper bar used for removing heat from the cold region of the TGP was cooled with liquid nitrogen. To prevent thermal communication with the ambient, the copper bars and TGP were insulated with two layers of $1/8$-in-thick butyl-coated PVC foam thermal insulation tape (McMaster–Carr, item 75875A662).

The temperature profile of the TGP was determined by monitoring thermocouples located at the hot and cold TGP interfaces. The heat flux through the TGP was determined by monitoring a third thermocouple that is located 1 cm away from the TGP interface on the hot copper bar, which provided power-transfer calculations using the known thermal conductivity of copper. As shown in Fig. 8, experiments were conducted at the following four separate fixed input temperatures: 97.5 °C, 100.7 °C, 105.4 °C, and 112.3 °C. The resulting power transfer through the TGP was 4.0, 4.8, 7.2, and 6.4 W, respectively. Once a fixed temperature was applied to the hot side of the TGP, the system was allowed to achieve a steady state over 15 min before measurements were taken. TGP thermal conductivity was calculated using the measured power transfer, heat source (copper block) dimensions (0.5 cm × 2 cm), and TGP dimensions (height is 0.6 mm, width is 3.0 cm, and length is 3.0 cm). Thermal paste (OMEGATHERM OT-201 Series) was used between the TGP and the hot and cold bars, and its resistance was considered in the TGP thermal conductivity calculations. The thermal resistance of the device is 7.19 K/W, and the contact resistance on each side of the contacts is 2.25 K/W. The maximum effective thermal conductivity is $k \sim 350$ W/m · K, which occurs at an input temperature of 105.4 °C. These values were calculated based on the aforementioned TGP dimensions with a length of 3 cm. The conductivity values that are shown in Fig. 8 are proportional to the length to be used. The effective conductivity values under different tilt angles and accelerations are important performance aspects of TGP devices for specific applications. These topics are under investigation and beyond the scope of this paper.

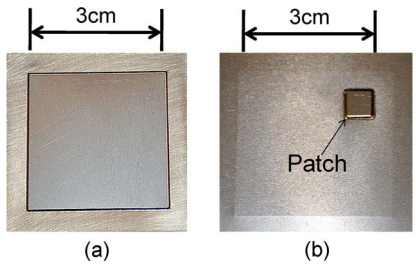

Fig. 9. Hermiticity data test. Panel (a) is the front side of a dummy TGP. Panel (b) shows the back side, which has a patch that is used to seal the hole used for charging water.

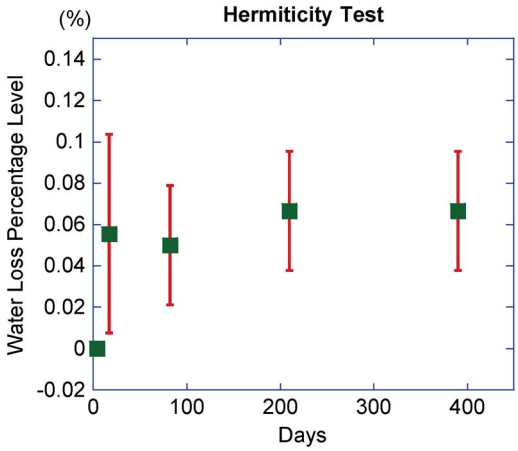

Fig. 10. Percentage loss of water as a function of time.

VII. Hermiticity Test

A 3 cm × 3 cm dummy TGP device was made with the same dimensions as Fig. 4 for hermiticity test. The device has a cavity of 200 μm × 3 cm × 3 cm, with standoffs inside to support. The net volume of the cavity is $\sim$170 μL. An amount of 60 μL of water was charged to the device at room temperature and atmospheric pressure before sealing the patch using laser welding technique, with argon as the shielding gas. The heat generated by laser welding is local due to the short pulse of the laser energy so that it does not reach the center area of the TGP device. The TGP device, as shown in Fig. 9, was then weighted with the Mettler Toledo lab scale (with 0.1-mg resolution), confirming that 60 ± 1 μL of water was enclosed.

The weight of the device was recorded before it was loaded into an oven where the device was kept at 100 °C in air ambient. The water loss was measured by weighting the device with Mettler Toledo lab scale with 0.1-mg resolution. The percentage of water loss is shown in Fig. 10. The device gives a 0.067% of water loss based on 60 μL of charged water for over a year term long at 100 °C in air.

VIII. Conclusion

A novel Ti-based flat heat pipe is developed by laser welding microfabricated Ti substrates. The device size is laterally 3 cm $\times$ 3 cm, with a thickness of 600 μm. A high-performance capillary wick was formed by etching 5-μm diameter pillars in titanium. The pillar array has a 10-μm center-to-center pitch and a height of 50 μm. The hydrophilic nature of the Ti pillars is increased by growing nanoscale ($\sim$200 nm) hairlike NST on the pillar surfaces. The wetting experiments show that the wick structure obeys Washburn dynamics and that it has a capillary velocity of $\sim$27.5 mm/s at a distance of 2 mm, which decreases to 5.5 mm/s at a distance of 10 mm. The wetting velocities increase 161% when the Ti pillars are coated with NST, as compared to uncoated Ti pillars.

The first-generation TGP device was constructed and found to have an effective thermal conductivity of 350 W/m $\cdot$ K, with a heat load of 7.2 W and with the hot side temperature of the TGP being 105.4 °C. The thermal conductivity value is proportional to the length to be used for calculation, based on the thermal resistance model. These data confirm the proof of concept of the Ti-based heat pipe. A dummy TGP with a cavity volume of $\sim$170 μL was used to test the hermiticity level of the laser packaging technique. The device gave a 0.067% of water loss based on $\sim$60 μL of charged water at 100 °C in air for over a year. We expect future generations of the Ti-based TGP to have significantly higher performance through the optimization of several design parameters and by eliminating noncondensable gases with a better optimized charging system.

References

[1] M. F. Aimi, M. P. Rao, N. C. MacDonald, A. S. Zuruzi, and D. P. Bothman, "High-aspect-ratio bulk micromachining of titanium," *Nat. Mater.*, vol. 3, no. 2, pp. 103–105, Feb. 2004.

[2] E. W. Washburn, "The dynamics of capillary flow," *Phys. Rev.*, vol. 17, no. 3, pp. 273–283, Mar. 1921.

[3] U. Vadakkan, G. M. Chrysler, and S. Sane, "Silicon/water vapor chamber as heat spreaders for microelectronic packages," in *Proc. 21st Annu. IEEE Semicond. Thermal Meas. Manage. Symp.*, 2005, pp. 182–186.

[4] H. Xie, H. Xie, A. Ali, and R. Bhatia, "The use of heat pipes in personal computers," in *Proc. 6th Intersoc. Conf. ITHERM*, 1998, pp. 442–448.

[5] T. Semenic and I. Catton, "Experimental study of biporous wicks for high heat flux applications," *Int. J. Heat Mass Transf.*, vol. 52, no. 21/22, pp. 5113–5121, Oct. 2009.

[6] H. de Bock, K. Varanasi, P. Chamarthy, T. Deng, A. Kulkarni, B. Rush, B. Russ, S. Weaver, and F. Gerner, "Experimental investigation of micro–nano heat pipe wick structures," in *Proc. ASME IMECE*, 2008, pp. 1–6.

[7] Q. Cai, C.-L. Chen, G. Xiong, and Z. Ren, "Explorations of carbon nanotube wick structure for high heat flux cooling," in *Proc. 2008 ASME Heat Transfer Summer Conf.*, Jacksonville, FL, pp. 293–297.

[8] R. Ranjan, J. Murthy, and S. Garimella, "Analysis of the wicking and thin-film evaporation characteristics of microstructures," *J. Heat Transf.*, vol. 131, no. 10, p. 101 001, Oct. 2009.

[9] Y. Chen, L. Melvin, S. Rodriguez, D. Bell, and M. Weislogel, "Capillary driven flow in micro scale surface structures," *Microelectron. Eng.*, vol. 86, no. 4–6, pp. 1317–1320, Apr.–Jun. 2009.

[10] E. R. Parker, M. F. Aimi, B. J. Thibeault, M. P. Rao, and N. C. MacDonald, "High-aspect-ratio inductively coupled plasma etching of bulk titanium for MEMS applications," in *Proc. 206th Meeting Electrochem. Soc.*, Honolulu, HI, 2004, p. 2580.

[11] C. O'Mahony, M. Hill, P. J. Hughes, and W. A. Lane, "Titanium as a micromechanical material," *J. Micromech. Microeng.*, vol. 12, no. 4, pp. 438–443, Jun. 2002.

[12] M. P. Rao, M. F. Aimi, and N. C. MacDonald, "Single-mask, three-dimensional microfabrication of high-aspect-ratio structures in bulk silicon using reactive ion etching lag and sacrificial oxidation," *Appl. Phys. Lett.*, vol. 85, no. 25, pp. 6281–6283, Dec. 2004.

[13] C. Ding, X. Huang, G. Gregori, E. R. Parker, M. P. Rao, D. R. Clarke, and N. C. MacDonald, "Development of bulk-titanium-based MEMS RF switch for harsh environment applications," in *Proc. ASME Conf.*, Orlando, FL, 2005, pp. 123–126.

Changsong Ding received the B.S. degree in naval architecture and ocean engineering from Shanghai Jiao Tong University, Shanghai, China, in 1996, and the M.S. and Ph.D. degrees in mechanical engineering from the University of California, Santa Barbara (UCSB), in 2003 and 2007, respectively, where he investigated and developed nonsilicon material micromachining and nanomodification-based 3-D microelectromechanical systems (MEMS).

From 1996 to 2001, he worked for several industrial companies including Delphi Automotive Systems Inc. and CNOOC, among others. He is currently an Assistant Project Scientist with the California NanoSystems Institute, UCSB. His current research focuses on bulk titanium-based MEMS including switch and flat heat pipe applications.

Gaurav Soni received the B.Tech. degree in mechanical engineering from the Indian Institute of Technology, New Delhi, India, and the M.S. and Ph.D. degrees in mechanical engineering from the University of California, Santa Barbara.

He is currently a Senior Analysis Engineer in the solar power generation industry. His research interests include fluid dynamics and heat transfer at both small and large scales.

Payam Bozorgi received the B.S. degree in mechanical engineering from Tehran Polytechnic University, Tehran, Iran, in 2000, and the M.S. degree in mechanical engineering from the University of Southern California, Los Angeles, in 2004. Since 2006, he has been working toward the Ph.D. degree at the University of California, Santa Barbara (UCSB), where he developed titanium-based microelectromechanical system packaging by using a micropulsed laser welding approach.

He is also a Research Assistant with the California NanoSystems Institute, UCSB.

Brian D. Piorek received the B.S. degree in chemical engineering and the Ph.D. degree in mechanical engineering from the University of California, Santa Barbara (UCSB), in 2002 and 2008, respectively, where he developed a microfluidic gas-phase chemical sensor technology.

He is a Visiting Research Scientist with the California NanoSystems Institute, UCSB, where he investigates the fundamental transport phenomena for microfluidic and chemical sensor applications. In 2008, he cofounded SpectraFluidics, Inc., Santa Barbara, where he currently serves as the Vice-President of Research and Development. Since 2004, he has also been with Gas Reaction Technologies, Inc., Santa Barbara.

Carl D. Meinhart received the Ph.D. degree from the University of Illinois at Urbana–Champaign, Urbana, in 1995.

While at the University of Illinois, his research involved the investigation of wall-bounded turbulent flows. Since 1996, he has been with the University of California, Santa Barbara, where he is currently a Professor of mechanical engineering and where his research has focused on developing and applying microresolution particle image velocimetry (micro-PIV) to study transport phenomena in microfluidic devices. His research group is involved in the development and analysis of bio-MEMS for immunoassays and molecular diagnostics and in the development of microfluidics for the detection of airborne molecules, such as explosives and narcotics.

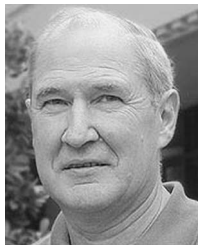

Noel C. MacDonald received the Ph.D. degree in electrical engineering from the University of California, Berkeley, in 1967.

He holds a joint professorial appointment in the Department of Mechanical and Environmental Engineering and the Department of Materials, University of California, Santa Barbara (UCSB), where he also holds the Fred Kavli Chair in Microelectromechanical Systems Technology. He was an Acting Assistant Professor at the University of California, Berkeley, from 1967 to 1968, he was a member of the Technical Staff at Rockwell International Science Center, and he held management positions at Physical Electronics Industries, Inc., and Perkin-Elmer Company from 1968 to 1982. Before joining UCSB, he held the Acheson/Laibe Professorship in Engineering at Cornell University, Ithaca, NY, and he served as the Director of the Cornell Nanofabrication Facility and the Chairman of the School of Electrical Engineering, Cornell University. From 1997 to 1999, he served as the Director of the Microsystems Technology Office, Defense Advanced Research Projects Agency. In 2000, he was elected to the National Academy of Engineering for his contributions to the development of the scanning auger microprobe and micromachined microinstruments. He has written or coauthored over 100 papers and several book chapters. He holds 61 patents. His current research interests include advanced materials processing as well as interdisciplinary research for micro/nanoelectromechanical systems.